Journal of Magnetic Resonance 203 (2010) 316–322

Contents lists available at ScienceDirect

Journal of Magnetic Resonance

journal homepage: www.elsevier.com/locate/jmr

Communication

Estimating quadrupole couplings of amide deuterons in proteins from direct measurements of ^{2}H spin relaxation rates

Devon Sheppard, Vitali Tugarinov *

Department of Chemistry and Biochemistry, University of Maryland, College Park, MD 20742, USA

ARTICLE INFO

Article history:
Received 4 November 2009
Revised 15 December 2009
Available online 24 December 2009

Keywords:
Deuterium relaxation
Amide deuteron
Hydrogen bond
Quadrupolar coupling

ABSTRACT

The measurements of longitudinal and transverse ^{2}H spin relaxation rates of backbone amide deuterons (D^N) in the [U–^{13}C,^{15}N]-labeled protein ubiquitin show that the utility of amide deuterons as probes of backbone order in proteins is compromised by substantial variability of D^N quadrupolar coupling constants (QCC) from one amide site to another. However, using the dynamics parameters of ^{15}N–^{2}H bond vectors evaluated from ^{15}N relaxation data, site-specific QCC values can be estimated directly from D^N R_1 and R_2 rates providing useful information on hydrogen bonding in proteins. In agreement with previous indirect scalar relaxation-based measurements, the D^N QCC values estimated directly from R_1 and R_2 ^{2}H relaxation rates correlate with the inverse cube of the X-ray structure-derived hydrogen bond distances in ubiquitin: $QCC = (232 \pm 2.3) + (118 \pm 17)\ \sum_i(\cos\alpha)r_i^{-3}$ where r is the inter-nuclear hydrogen bond distance in ångströms, and α is the N–D···O$_i$ angle.

1. Introduction

Deuterium nuclei are particularly 'convenient' probes of molecular dynamics in proteins. ^{2}H relaxation is dominated by quadrupolar interaction [1], and the knowledge of only a single parameter, the anisotropy of ^{2}H quadrupolar tensor or quadrupole coupling constant (QCC), is needed for the interpretation of ^{2}H relaxation data in terms of order parameters of bond vector motions. NMR methodology for the measurement of ^{2}H relaxation rates have been under intensive development in the past 15 years [2–4]. Previously, ^{2}H relaxation measurements in proteins have been confined to side-chain deuterons — primarily methyl groups of the $^{13}CH_2D$ [2,3,5,6] or $^{13}CHD_2$ [7] variety, ^{13}CHD groups [8], or ^{15}NHD moieties of asparagine and glutamine side-chains [9]. The availability of increasingly sensitive NMR instrumentation allows the quantification of ^{2}H relaxation rates at protein backbone sites. Very recently, we developed NMR methodology that extends the utility of deuterium as a probe of motions to α positions (D^α) in the backbones of [U–^{15}N,^{13}C,^{2}H]-labeled proteins [10]. Using the D^α ^{2}H-derived measures of backbone order, it has been shown that in agreement with 1-μs molecular dynamics simulations, the backbone C^α–D^α bond vectors are motionally distinct from the amide N–H bond vectors, with average order parameters of C^α–D^α fluctuations slightly higher than their N–H counterparts [10].

Here, we explore the utility of amide deuterons (D^N) as spin probes of backbone ordering in proteins. An NMR experiment is developed for the measurement of D^N R_1 and R_2 relaxation rates in the backbone amide ^{15}N–^{2}H spin pairs. The quantification of ^{2}H relaxation rates at D^N backbone positions of the [U–^{15}N,^{13}C]-labeled protein human ubiquitin at 27 °C is feasible with an accuracy sufficient for (i) the derivation of the global molecular reorientation tensor, and (ii) direct estimation of site-specific D^N QCC values. In contrast to D^α QCC, amide deuteron QCC values are highly variable and inversely dependent on the distance to the nearest hydrogen bonding partner [11]. The D^N QCC values calculated directly from D^N R_1 and R_2 relaxation rates are correlated with hydrogen bond lengths in the crystallographic structure of ubiquitin: $QCC = 232 + 118\sum_i(\cos\alpha)r_i^{-3}$ where r is the inter-nuclear hydrogen bond distance in ångströms, and α is the N–D···O$_i$ angle. These results are compared to the values obtained earlier via indirect measurements using scalar relaxation of the second kind [11,12].

2. Results and discussion

2.1. The measurement of ^{2}H relaxation rates of backbone amide deuterons

Amide deuteron $R_2(D_z)$ and $R_1(D_+)$ rates have been measured using the insets A and B, respectively, of the 2D HA(CACO)ND pulse-scheme shown in Fig. 1. The pulse-scheme is derived from the 3D HACA(CO)N experiment [13,14] with the addition of the element enclosed in the dashed rectangle (Fig. 1) that ensures the transfer of magnetization from the amide ^{15}N to the attached

* Corresponding author. Address: Biomolecular Sci. Bldg./CBSO, Department of Chemistry and Biochemistry, University of Maryland, College Park, MD 20742, USA. Fax: +1 301 3140386.
E-mail address: vitali@umd.edu (V. Tugarinov).

1090-7807/$ - see front matter © 2009 Elsevier Inc. All rights reserved.
doi:10.1016/j.jmr.2009.12.020

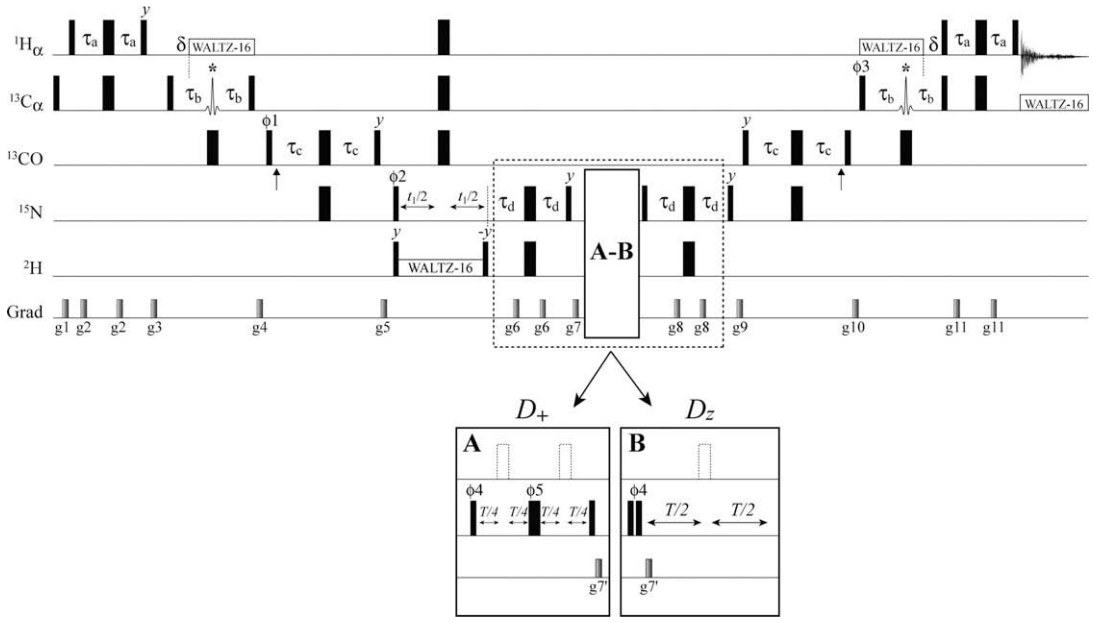

Fig. 1. The pulse-scheme for the measurement of $R^Q(D_+)$, $R^Q(D_z)$ rates of amide deuterons (D^N) in [U–^{15}N,^{13}C]-labeled proteins. Insets (A) and (B) correspond to the measurement of $R_2 = R^Q(D_+)$ and $R_1 = R^Q(D_z)$, respectively. All narrow (wide) rectangular pulses were applied with the flip angles of 90°(180°) along the *x*-axis unless indicated otherwise. The ^{1}H(^{2}H; ^{15}N) carriers are positioned at 4.7(8.0; 119) ppm. The ^{13}C carrier is placed at 57 ppm, switched to 177 ppm before the 90° ^{13}CO pulse applied with phase φ1, and returned to 57 ppm before the 90° $^{13}C^\alpha$ pulse applied with phase φ3. ^{2}H and ^{13}C WALTZ-16 [38] decoupling is applied with 0.9 and 2.0 kHz field strengths, respectively, while ^{1}H WALTZ-16 [38] decoupling is applied with a 7 kHz field strength. All ^{1}H, ^{2}H and ^{15}N pulses are applied with maximum possible power, while 90°(180°) ^{13}C pulses are applied with a field strength of $\Delta/\sqrt{15}(\Delta/\sqrt{3})$ where Δ is the difference (in Hz) between the $^{13}C^\alpha$ and ^{13}CO chemical shifts [39]. Vertical arrows at the beginning and the end of $2\tau c$ periods indicate the position of the ^{13}CO Bloch–Siegert shift compensation pulses [39]. $^{13}C^\alpha$ shaped pulses in the middle of $2\tau b$ periods (marked with asterisks) are implemented as $^{13}C^\alpha$-selective 1.55-ms long RE-BURP [40] pulses (600 MHz) centered at 56 ppm by phase modulation of the carrier [41,42] and cover the range of $^{13}C^\alpha$ resonances of all residues except glycines. ^{15}N pulses shown with open dashed rectangles in insets (A) and (B) are optional. Delays are: $\tau_a = 1.8$ ms; $\tau_b = 4.5$ ms; $\tau_c = 12.5$ ms; $\tau_d = 6.0$ ms; $\delta = 3.6$ ms; *T* is the variable relaxation delay. The $2\tau d$ period is shorter than $1/4^1J_{N-D}$ to maximize the magnetization transfer in the presence of ^{2}H relaxation [9]. The phase-cycle is: φ1 = *x*, −*x*; φ2 = 2(*x*), 2(−*x*); φ3 = 4(*x*), 4(−*x*); φ4 = 8(*x*), 8(−*x*); φ5 = *x*, −*x*, *y*, −*y* (inset A only); rec. = 2(*x*, −*x*), 4(−*x*, *x*), 2(*x*, −*x*) (if inset A is used) and rec. = *x*, −*x*, −*x*, *x*, 2(−*x*, *x*, *x*, −*x*), *x*, −*x*, −*x*, *x* (inset B). Quadrature detection in t_1 is achieved via the States-TPPI incrementation of phase φ2 [43]. Durations and strengths of pulsed-field gradients in units of (ms; G/cm) are: g1 = (1; 15); g2 = (0.25; 5); g3 = (1.2; 12); g4 = (0.5; 8); g5 = (0.6; 10); g6 = (0.3; 5); g7 = (0.9; 15); g8 = (0.35; 5); g9 = (0.5; 12); g10 = (1.0; 10); g11 = (0.3; 5); g7′ = (0.7; 15). All ^{2}H relaxation measurements were performed on a 600 MHz Bruker Avance III spectrometer equipped with a room temperature triple-resonance *z*-gradient probe using a [U–^{15}N,^{13}C]-labeled sample of human ubiquitin. The sample was 3.2 mM in protein concentration, dissolved in a 20 mM 99.9% D_2O sodium phosphate buffer (uncorrected pH reading of 6.8) containing 0.03% NaN_3. The data sets comprised [512; 64] complex points in the [$^1H_{\alpha,i-1}$; $^{15}N_i$] dimensions with corresponding acquisition times of [64 ms; 38 ms]. A recovery delay of 1 s was used along with 256 scans/FID giving rise to net acquisition times of ∼10 h/experiment. D^N $R^Q(D_+)$ rates (inset A) of amide deuterons were recorded with parametrically varied delays *T* of (0.002; 0.2; 0.4; 0.6; 0.8; 1.0; 1.2) ms, while $R^Q(D_z)$ rates (inset B) were recorded with parametrically varied delays *T* of (0.002; 1.0; 2.0; 3.0; 4.0; 6.0; 8.0) ms. All NMR spectra were processed using the NMRPipe/NMRDraw programs and associated software [44]. Rates were obtained by fitting peak intensities to a single exponential function of the form $I = I_0 exp(-RT)$, where *I* is the measured intensity and *R* is the relaxation rate. Errors in peak intensities have been estimated from duplicate measurements or from the noise-floor level of the spectra, whichever was the highest, and subsequently propagated to the errors in the extracted rates using Monte-Carlo analysis [45]. In principle, the correlations corresponding to the residues following glycines can be quantified in a separate measurement with delay δ set to 1.8 ms and the $^{13}C^\alpha$-selective RE-BURP pulses adjusted to a 4 ms length (600 MHz) and centered at 45 ppm by phase modulation of the carrier. In practice, however, such experiments are ∼4-fold less sensitive providing only approximate estimates of ^{2}H R_1 and R_2 rates for the amide positions following glycines.

D^N nuclei and back. The magnetization flow can be summarized as follows,

$$^1H_{\alpha,i-1} \rightarrow {}^{13}C_{\alpha,i-1} \rightarrow {}^{13}CO_{i-1} \rightarrow {}^{15}N_i(t_1) \rightarrow D_{N,i}(T) \rightarrow {}^{15}N_i \rightarrow {}^{13}CO_{i-1} \rightarrow {}^{13}C_{\alpha,i-1} \rightarrow {}^1H_{\alpha,i-1}(t_2), \quad (1)$$

where the transfer from one spin to the next is achieved via one-bond scalar couplings and t_1, t_2 are evolution and acquisition times, respectively. A series of two-dimensional data sets is recorded as a function of the parametrically varied relaxation delay *T*. The cross-peaks obtained at the frequencies ($\omega_{H\alpha,i-1}$; ω_{Ni}) decay with the relaxation rates of α-deuterons belonging to residue *i*, $D_{N,i}$ (Eq. (1)). The pulse-scheme differs from other implementations of the 2D HACA(CO)N experiment [11,15] in that the pulses in the center of the $2\tau_b$ period (marked with asterisks in Fig. 1) are implemented as $^{13}C^\alpha$-selective pulses that refocus $^{13}C^\alpha$ resonances of all residues except glycines. As a result, $^1J_{C\alpha C\beta}$ couplings are refocused in the end of the time period $2\tau_b$ in all amino-acids except serines whose $^{13}C^\beta$ magnetization is (partially) inverted by $^{13}C^\alpha$-selective pulses. Therefore, correlations corresponding to the ($\omega_{H\alpha,i-1}$; ω_{Ni}) frequencies of the residues following glycines are not observed, while those following serines are usually attenuated. A region of the 2D HA(CA-CO)ND spectrum recorded on the [U–^{13}C,^{15}N]-labeled human ubiquitin in D_2O at 27 °C using the pulse scheme of Fig. 1 (inset A, $T = 0$) is shown in Fig. 2a. Fig. 2b and c illustrate typical D_z and D_+ exponential decay curves for a pair of residues in ubiquitin. The evolution of ^{15}N chemical shifts during t_1 can be implemented in a semi-constant time manner [16]; however, due to slow relaxation of the transverse ^{15}N magnetization in ^{15}N–^{2}H pairs in the presence of deuterium decoupling [17], the gains in sensitivity resulting from this modification are marginal at best.

2.2. ^{2}H relaxation rates of amide deuterons

The pulse-scheme of Fig. 1 effectively measures the relaxation rates of magnetization terms $N_zC'_zC^\alpha_z[D]$, where [*D*] is any deuterium spin operator and A_z is a longitudinal spin operator of nucleus A. As it is the case in the previous deuterium relaxation studies [2,3,9,18], it is straightforward to show that to an excellent approximation $R(N_zC'_zC^\alpha_z[D]) = R(N_zC'_zC^\alpha_z) + R[D]$, and to obtain 'pure' amide deuterium relaxation rates it is sufficient to

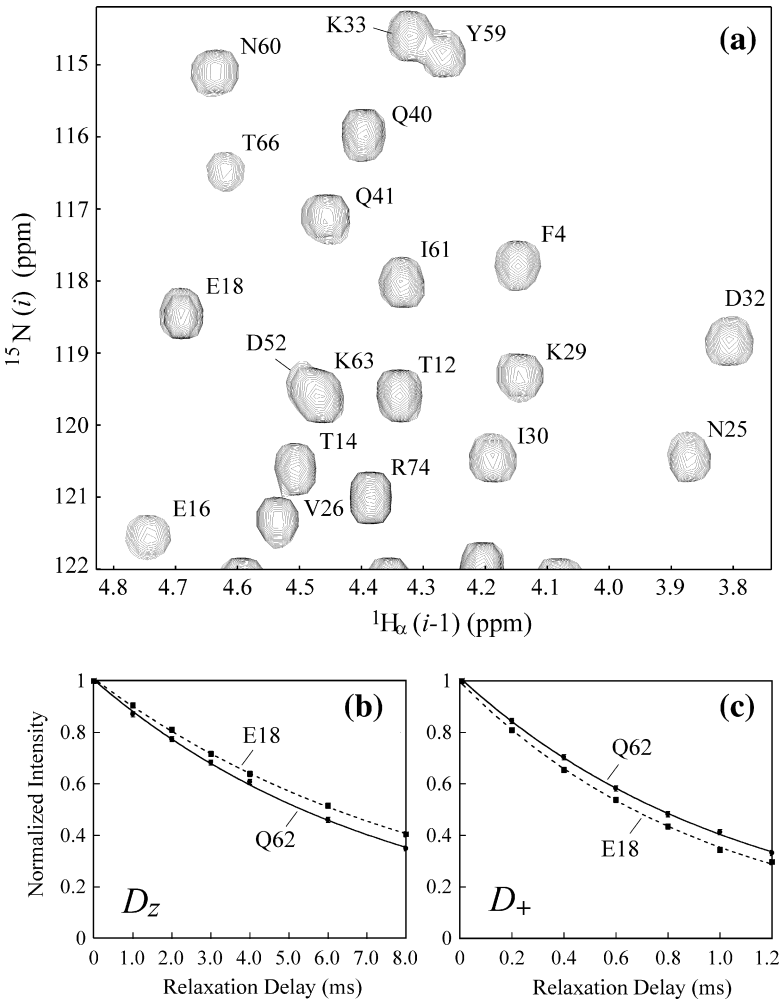

Fig. 2. (a) A region of the $^{1}H_{\alpha,i-1}$–$^{15}N_i$ correlation map of the [U–^{15}N,^{13}C]-labeled ubiquitin (27 °C; 600 MHz) acquired as the first measurement point in the experiment of Fig. 1 (inset A, $T = 0$). Assignments of cross-peaks are shown according to their ^{15}N frequencies. Note that peak positions are shifted upfield by ~0.7 ppm in the ^{15}N dimension compared to ^{15}N–^{1}H amides as a result of a one-bond deuterium isotope shift [12,15,46]. Typical single-exponential decay curves of (b) D_z, and (c) D_+ magnetization are shown for the amide deuterons of Glu^{18} (dashed curves) and Gln^{62} (solid curves) of ubiquitin.

subtract $R(N_zC'_zC^{\alpha}_z)$ from the rates obtained in the experiment of Fig. 1. In practice, however, the decay rates of the three-spin order $N_zC'_zC^{\alpha}_z$ (measured separately using a pulse-scheme derived from the 2D HA(CACO)N experiment) are very small compared to $R(N_zC'_zC^{\alpha}_z[D])$. For example, the $R(N_zC'_zC^{\alpha}_zD_+)$ and $R(N_zC'_zC^{\alpha}_zD_z)$ rates vary between 383 and 1435 s^{-1} and between 113 and 177 s^{-1}, respectively, while the rates $R(N_zC'_zC^{\alpha}_z)$ are in the range between 2.8 and 3.9 s^{-1}. Although the $R(N_zC'_zC^{\alpha}_z)$ rates are usually within measurement errors of D^N $R(N_zC'_zC^{\alpha}_zD_+)$ and $R(N_zC'_zC^{\alpha}_zD_z)$, to avoid introduction of systematic errors the $R(N_zC'_zC^{\alpha}_z)$ values have been subtracted from D^N $R(N_zC'_zC^{\alpha}_z[D])$ rates on a residue-specific basis.

The relaxation rates of ^{2}H transverse and longitudinal magnetization are given by [1],

$$R^{Q}(D_+) = R^{Q}_2 = \frac{\pi^2}{20}\left(1+\frac{\eta^2}{3}\right)\left(\frac{e^2qQ}{h}\right)^2 [9J(0)+15J(\omega_D)+6J(2\omega_D)] \quad (2)$$

$$R^{Q}(D_z) = R^{Q}_1 = \frac{3\pi^2}{10}\left(1+\frac{\eta^2}{3}\right)\left(\frac{e^2qQ}{h}\right)^2 [J(\omega_D)+4J(2\omega_D)] \quad (3)$$

where (e^2qQ/h) is the quadrupolar coupling constant, QCC (in Hz), $J(\omega_D)$ is the spectral density function evaluated at ω_D frequency, and η is the asymmetry parameter of the ^{2}H electric field gradient tensor. The asymmetry values η in amide deuterons are typically $\leqslant$0.22 [19], and the terms $\left(1+\frac{\eta^2}{3}\right)$ in Eqs. (2) and (3) may contribute maximum ~1.6% to D^N ^{2}H relaxation rates. This contribution is normally lower than the errors in D^N ^{2}H rate measurements, and η has been assumed to be zero in all calculations. To a good approximation, the principal axis of the axially symmetric electric field gradient tensor is parallel to the direction of the N–D bond [20,21]. Then, the main characteristic of the electric field gradient tensor entering the expressions for relaxation rates in Eqs. (2) and (3) is its anisotropy, (e^2qQ/h) = QCC. QCC values of amide deuterons in proteins are highly variable [11] depending on the presence and strength of hydrogen bonds involving the amide group in question (*vide infra*). Eqs. (2) and (3) are rigorously applicable to an isotropically tumbling molecule: in the case of a finite asymmetry value η and anisotropic molecular tumbling, different spectral densities should be formulated for each orthogonal component of the electric field gradient tensor. The rigorous treatment can be found in Chung et al. [22]. Once the electric field gradient tensor is assumed to be axially symmetric ($\eta = 0$) and collinear with the direction of the ^{15}N–D bond as above, the following Lipari–Szabo model-free spectral density function for the axially symmetric molecular tumbling can be used [23–25],

$$J(\omega) = S^2\left(\frac{A_1\tau_1}{1+(\omega\tau_1)^2}+\frac{A_2\tau_2}{1+(\omega\tau_2)^2}+\frac{A_3\tau_3}{1+(\omega\tau_3)^2}\right) + \left(1-S^2\right)\frac{\tau'}{1+(\omega\tau')^2} \quad (4)$$

where S is the generalized order parameter describing the fluctuations of N–D bond vectors, $A_1 = (3/4)\sin^4(\beta)$, $A_2 = 3\sin^2(\beta)\cos^2(\beta)$, $A_3 = [(3/2)\cos^2(\beta) - 0.5]^2$, $\tau_1 = (4D_{||} + 2D_\perp)^{-1}$, $\tau_2 = (D_{||} + 5D_\perp)^{-1}$, $\tau_3 = (6D_\perp)^{-1}$, $D_{||}$ and $D_\perp$ are the parallel and perpendicular components of the molecular diffusion tensor, β is the angle between the N–D bond vector (assumed collinear with the N–H bond) and the unique diffusion axis, and $1/\tau' = 1/\tau_f + 1/\tau_{c,eff}$, where the effective correlation time of overall rotation $\tau_{c,eff} = (2D_{||} + 4D_\perp)^{-1}$, and τ_f is the correlation time of fast local motions. Direction cosines for N–H(D) vectors of human ubiquitin have been obtained from the protonated X-ray structure with the PDB accession code 1ubq [26].

Fig. 3 shows the profiles of the $R^Q(D_z)$ (Fig. 3a) and $R^Q(D_+)$ (Fig. 3b) rates of amide deuterons in ubiquitin at 27 °C (600 MHz). The $R^Q(D_z)$ and $R^Q(D_+)$ profiles of D^α deuterons of ubiquitin quantified previously under the same experimental conditions [10] are included in the plots for comparison. The respective average D^N $R^Q(D_+)$ and $R^Q(D_z)$ rates are 1097 and 132 s^{-1}. Although the motional characteristics of N–D and C^α–D^α bond vectors in proteins are quite similar [10], D^N $R^Q(D_+)$ rates are 1.84-fold higher on average than their D^α counterparts (Fig. 3b). This is the direct consequence of (i) ~1.25-fold higher QCC values of amide deuterons (note the quadratic dependence of the rates on QCC in Eqs. (2) and (3)), and (ii) 1.23-fold higher viscosity of D_2O vs. H_2O at 27 °C [27] leading to proportionately higher values of $\tau_{c,eff}$ in the present study. Note that D^N $R^Q(D_z)$ rates are only 1.24-fold higher on average than D^α $R^Q(D_z)$ rates (Fig. 3a) because in addition to quadratic dependence on QCC, the $R^Q(D_z)$ rates of amides with restricted internal motions are approximately inversely proportional to $\tau_{c,eff}$ (Eqs. (3) and (4)). It is also apparent from Fig. 3 that D^N $R^Q(D_+)$ and $R^Q(D_z)$ rates are significantly more variable from one protein site to another in comparison to their D^α counterparts: relative r.m.s.d. from the mean $D^N(D^\alpha)$ rate calculated for the same subset of residues is ±14.9(8.2)% and ±10.8(6.1)% for $R^Q(D_+)$ and $R^Q(D_z)$, respectively. This variability oftentimes masks the variations in rates arising from different degrees of backbone order (S^2_{NH}) and/or different time-scales of motional processes. Therefore, quantitative interpretation of D^N R_2 and R_1 rates in terms of motional characteristics is highly unreliable without the knowledge of residue-specific QCC values.

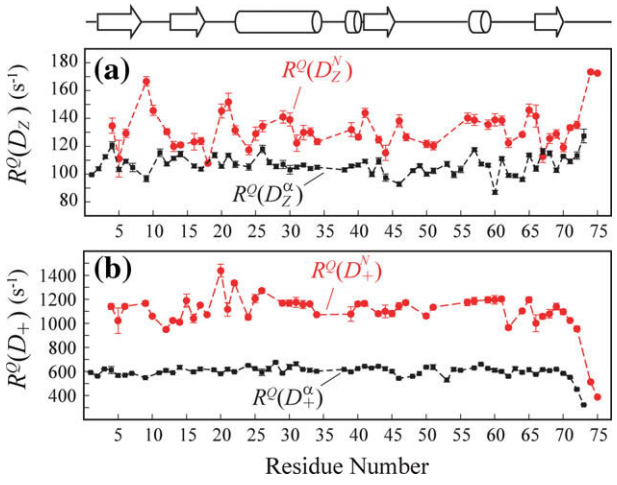

Fig. 3. The plots of D^N (shown with red filled circles) and D^α (black filled rectangles) relaxation rates as a function of the protein sequence: (a) D^N and D^α $R^Q(D_z)$, and (b) D^N and D^α $R^Q(D_+)$ rates (s^{-1}) obtained in human ubiquitin at 27 °C (600 MHz). D^α relaxation rates have been measured as described previously [10]. Schematic representation of the secondary structure of ubiquitin is shown on top: β-sheets are depicted with arrows, while α-helices are represented with cylinders.

Taking into account different sample concentrations used into the two studies, we estimate that D^N relaxation measurements using the scheme of Fig. 1 are approximately 2.5-fold less sensitive compared to the HN(COCA)-based ^2H relaxation measurements at D^α sites [10]. This is a direct consequence of (i) smaller $^1J_{ND}$ coupling constants (~14 Hz) compared to $^1J_{C\alpha D\alpha}$ (~22 Hz) leading to longer magnetization transfer periods to and from amide ^2H, and (ii) faster ^2H spin flipping rates in the ^{15}N–D spin systems during these magnetization transfer steps (two $2\tau_d$ periods in the scheme of Fig. 1). It is noteworthy that, in general, a total of five relaxation rates can be measured per deuteron: in addition to 'rank-1' coherences (D_+ and D_z), the relaxation rates of 'rank-2' elements ($D_+D_z + D_zD_+$, $3D_z^2 - 2$ and D_+^2) can be quantified at the same ^2H positions [3]. In fact, one of the principal advantages of ^2H spin relaxation stems from the possibility to verify the consistency of the five ^2H rates [28] prior to analysis in terms of motional parameters [3]. However, the measurements of 'rank-2' elements of backbone deuterons are significantly less sensitive than their 'rank-1' counterparts [10,18] — especially so in the case of ^2H relaxation measurements at D^N positions where prolonged periods of $^1J_{N-D}$ evolution and high ^2H R_1 rates lead to very substantial sensitivity losses. Thus, reliable ^2H 'rank-2' rate measurements at D^N sites were not feasible within a reasonable experimental time frame. Likewise, the measurements of D^N ^2H rates in ubiquitin at 10 °C proved too insensitive for further quantitative analysis.

Although ^2H relaxation rates of 'rank-1' coherences considered here are normally not affected by contributions from chemical exchange, amide deuterons represent a special case in this regard because they can exchange with the solvent. For example, one could envisage a solvent-exposed amide deuteron exchanging fast with the bulk solvent (with rates on the order of 10–50 s^{-1}). This exchange process would still be in the slow regime on the chemical shift time-scale and could potentially affect D^N $R^Q(D_+)$ and $R^Q(D_z)$ rates (note that amide deuterons are not detected directly in the experiment of Fig. 1). However, intrinsic exchange rates of amide deuterons in a protein at the pH(pD) = 6.8(7.2) of this study are ~3 s^{-1} [29,30] and are expected to be much lower for (buried) hydrogen-bonded amides. No sizable solvent exchange contributions have been detected in this work: the average $R^Q(D_+)$ and $R^Q(D_z)$ rates of the 6 non-hydrogen-bonded, non-mobile amide deuterons with more than 20% solvent exposure in ubiquitin are *lower* than the average rates by 9% and 5%, respectively (in most of the cases due to lower D^N QCC values resulting from hydrogen bonding with water; *vide infra*).

2.3. Derivation of overall diffusion tensor parameters from D^N relaxation rates

The ratio of ^2H R_2 and R_1 rates, $R_2/R_1 = R^Q(D_+)/R^Q(D_z)$, is to a good approximation independent of the amplitude and time-scale of rapid internal motions [31,32]. Furthermore, the ^2H R_2/R_1 ratios are not affected by the variability of D^N QCC values, as ^2H R_1 and R_2 rates share the same quadratic dependence on QCC (Eqs. (2) and (3)). Therefore, ^2H R_2/R_1 ratios can serve as a good measure of the rate at which N–D bond vectors reorient with the global molecular tumbling. After exclusion of all mobile residues (^1H–^{15}N NOE < 0.7), and using the procedure detailed elsewhere [10,18,32], the following diffusion tensor parameters have been derived from D^N $R^Q(D_+)/R^Q(D_z)$ ratios for ubiquitin in D_2O: ($\tau_{c,eff}$ = 5.28 ± 0.03 ns; $D_{||}/D_\perp$ = 1.24 ± 0.03; θ = 14 ± 6°; φ = −172 ± 40°), where the polar angles θ and φ that determine the orientation of the unique axis of the global diffusion tensor, are specified in the inertial coordinate frame. These values agree reasonably well with the ^{15}N relaxation-derived parameters [10],

after $\tau_{c,eff}$ in the latter is corrected for the 1.23-fold higher viscosity of D_2O at 27 °C [27]: ($\tau_{c,eff}$ = 5.12 ± 0.01 ns; $D_{||}/D_{\perp}$ = 1.18 ± 0.02; θ = 6 ± 2°; φ = −16 ± 4°). A fit to a fully anisotropic diffusion tensor [32] was not warranted because of relatively high errors in extracted D^N R^Q[D] relaxation rates (~2.1% on average).

The extraction of global diffusion tensor parameters from D^N ^2H rates is less reliable than from ^{15}N or even D^{α} ^2H data [10]. The difference of 19° between the ^{15}N- and D^N ^2H-derived orientations of the principal diffusion axes probably reflects significantly lower accuracy with which the D^N relaxation rates can be quantified. However, the analysis of the relaxation data in terms of D^N QCC values (see below) is stable with respect to the orientation of the principal axis of the diffusion tensor.

2.4. Direct estimation of D^N QCC values from $R^Q(D_+)$ and $R^Q(D_z)$ rates

As described above, the interpretation of amide deuteron $R^Q(D_+)$ and $R^Q(D_z)$ rates in terms of order parameters of N–D bond vector motions is problematic because of the uncertainties in residue-specific D^N QCC values. However, the measured rates can be useful for direct evaluation of site-specific QCC values provided that the site-specific parameters of local motions (S^2_{NH}; τ_f) are known from ^{15}N relaxation studies of ^{15}N–^1H amides. Because of twice higher mass of deuterons, the amplitudes of local motions (S^2) may be affected by the ^1H-to-^2H substitution due to zero-point vibrational effects and a noticeable contribution of librational motions to S^2 [33,34]. This may also be true for the time-scales of local motions (τ_f). Nevertheless, here we assume that these changes are relatively small. In fact, the directly measured ^{15}N rates in ^{15}N–D spin pairs of protein G have been found in good agreement with theoretical predictions based on the microdynamic parameters (S^2_{NH}; τ_f) obtained from ^{15}N data in ^{15}N–^1H amides [17]. In addition, the dynamics of the vast majority of residues in ubiquitin can be adequately described using the simplest form of the spectral density function of Eq. (4), where τ_f is assumed to have zero or negligible contribution [10,32].

Earlier, LiWang and Bax [11] determined the QCC values for the subset of 35 amide deuterons in ubiquitin using indirect measurements of the effect of scalar relaxation of the second kind [1] on the ^{15}N relaxation rates in backbone ^{15}N–^2H amide triplets. A conceptually similar but technically different approach was adopted by Boyd et al. [12] for QCC measurements in ^{15}NHD moieties of asparagine and glutamine side chains. The approaches using scalar relaxation are also predicated upon the knowledge of exact residue-specific dynamics parameters (S^2_{NH}; τ_f). Moreover, the determined values of QCC are strongly dependent upon the chosen value of $^1J_{ND}$. The exact value of this scalar coupling is difficult to measure; usually, $^1J_{NH}$ couplings are accurately measured and subsequently scaled by the factor (γ_D/γ_H), where γ_i is the gyromagnetic ratio of nucleus *i*. As an illustration, we have plotted the scalar relaxation-derived QCC as a function of the adopted value of $|^1J_{ND}|$ in Fig. 4. It is apparent from the plot that an error in $^1J_{ND}$ as small as 0.2 Hz can introduce an error of 4.5 kHz in QCC determination. The same error in QCC would arise from an error in S^2_{NH} of ~0.035 (Fig. 4; dashed line). Approximately the same errors are expected from the uncertainties in S^2_{NH} in the direct estimation of QCC used here.

Because of the same quadratic dependence of $R^Q(D_+)$ and $R^Q(D_z)$ on QCC (Eqs. (2) and (3)), any linear combination of ^2H R_1 and R_2 rates can be used for recalculation of QCC using the (S^2_{NH}; τ_f) values from ^{15}N-relaxation measurements performed under the same experimental conditions [10]. The recalculation of QCC using both the sum and the difference of $R^Q(D_+)$ and $R^Q(D_z)$ as well as best-fitting $R^Q(D_+)$ and $R^Q(D_z)$ rates using a single fitting parameter provided very similar results (pair-wise r.m.s.d. of the obtained QCC values in either case <2 kHz). The best results in terms of correlations with hydrogen bond lengths (*vide infra*) are, however, achieved using the sum of the rates whereby D^N QCC (in Hz) is obtained via the following expression:

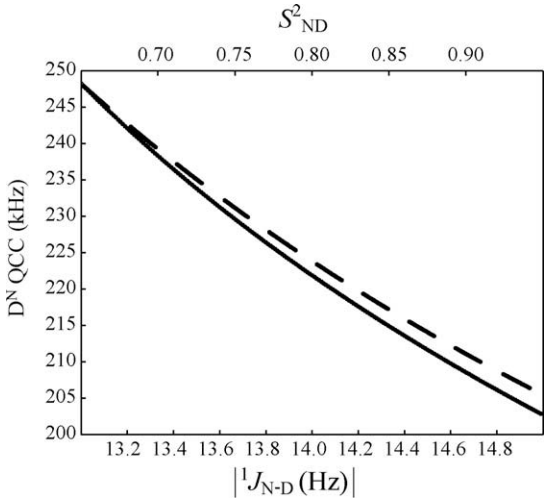

Fig. 4. Simulated dependence of the D^N QCC (*y*-axis), determined from the decay of ^{15}N magnetization in a ^{15}N–^2H triplet due to scalar relaxation of the second kind [11], on the absolute value of the one-bond scalar coupling constant, $|^1J_{N-D}|$, (*x*-axis, bottom; solid curve) and the squared order parameter of the N–D(H) bond vector motions, S^2_{NH}, (*x*-axis, top; dashed curve). The simulations of QCC determination have been performed using the classical description of the evolution of the ^{15}N–^2H triplet as described by LiWang and Bax [11] for an isotropically tumbling molecule with rotational correlation time τ_c = 5.2 ns and S^2_{NH} fixed at 0.88 (solid curve) and $^1J_{N-D}$ fixed at −14.4 Hz (dashed curve).

$$\mathrm{QCC} = \frac{2}{\pi}\left(\frac{(R^Q_{1,exp} + R^Q_{2,exp})}{\frac{1}{5}\sum_i a_i J(\omega_i)}\right)^{\frac{1}{2}} \tag{5}$$

where $R^Q_{1,exp}$ and $R^Q_{2,exp}$ are experimental $R^Q(D_z)$ and $R^Q(D_+)$ rates, and $\sum_i a_i J(\omega_i) = [9J(0) + 21J(\omega_D) + 30J(2\omega_D)]$. The sign of QCC can not be determined from Eq. (5) and is assumed to be positive. The QCC values obtained from Eq. (5) are plotted versus the protein sequence in Fig. 5a (red circles). For comparison, we have included the QCC values obtained by LiWang and Bax [11] on the same plot (black triangles). The sources of discrepancies between the two QCC measurements are manifold and may arise from: (i) different sample conditions used in the two studies (25 °C; pH = 4.7 in LiWang and Bax [11] and 27 °C; pH = 6.8 in this work), and (ii) the intrinsic inaccuracies of both QCC determination methods due to uncertainties in global and local dynamics parameters (both methods) and $^1J_{ND}$ couplings (the scalar relaxation- based method). The D^N QCC values obtained from Eq. (5) are on average 5.7 kHz (2.7%) higher than those reported in [11]. However, a semi-quantitative agreement between the two measurements can be noted. For example, the residue with the lowest QCC in both studies (208.9 and 199.7 kHz, respectively) is Glu^{18} whose amide deuteron is hydrogen bonded to carboxyl of Asp^{21}, confirming that hydrogen bonding to charged carboxyl oxygens decreases the D^N QCC more than to backbone carbonyls. The largest QCC values are obtained for the amides weakly hydrogen-bonded to hydroxyl oxygens of threonines and serines: Thr^{20} (247.5 kHz), Thr^9 (242.8 kHz), Thr^{22} (234.3 kHz) weakly hydrogen bonded to Thr^{20}, Thr^7, and Thr^{22} Oγ oxygens, respectively, whereas the largest QCC value obtained by LiWang and Bax is for Thr^9 (236 kHz).

Practically all amides in the crystal structure of ubiquitin are either involved in one or two hydrogen-bonds or are exposed to the solvent. Normally, hydrogen bonding reduces the values of D^N QCC (see below). Interestingly, the QCC values of many non-hydrogen-bonded amides with solvent exposure of more than 20% have

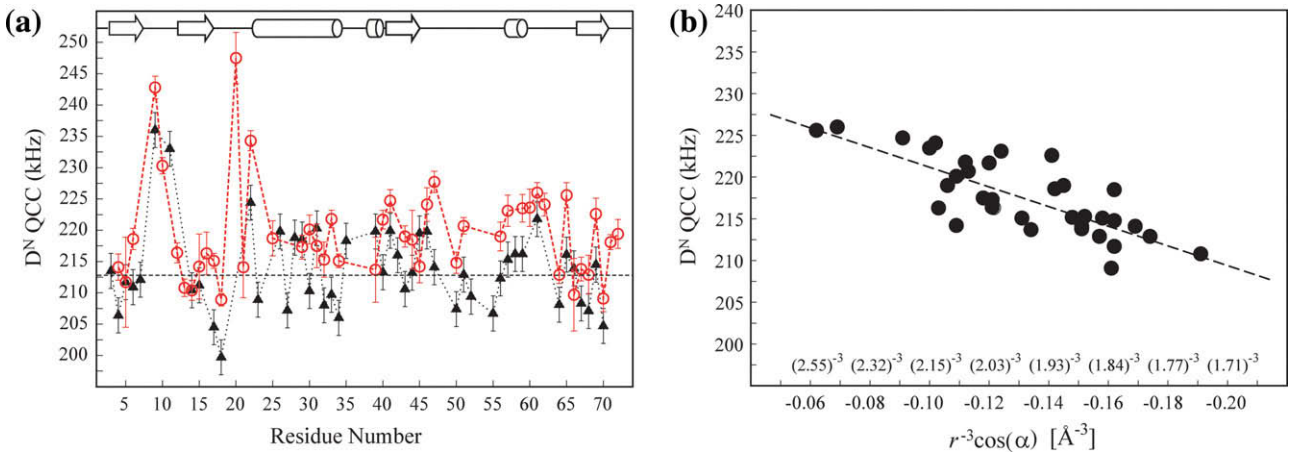

Fig. 5. (a) D^N QCC values derived from the sum of amide deuteron relaxation rates, $R_1^Q(D_z) + R_2^Q(D_+)$, in ubiquitin (27 °C) are shown with open red circles and plotted as a function of the protein sequence. D^N QCC values obtained earlier from the scalar relaxation of the second kind by LiWang and Bax [11] are shown with filled black triangles. A uniform error of 2.8 kHz is assumed for the QCC values of LiWang and Bax [11], whereas for the D^N QCC values estimated from Eq. (5), the errors are propagated from uncertainties in $R_1^Q(D_z)$ and $R_2^Q(D_+)$ rates. QCC values for Leu[15] and Phe[45] have been obtained from $R_2^Q(D_+)$ rates only. The dashed horizontal line corresponds to the amide deuteron QCC (212.6 kHz) obtained by Gerald et al. [20] in a single-crystal solid state NMR study of *N*-acetyl-D,L-valine. Schematic representation of the secondary structure of ubiquitin is shown on top: β-sheets are shown with arrows, while α-helices are represented with cylinders. (b) Correlation of D^N QCC values and inverse cube backbone–backbone and backbone–water hydrogen bond distances (Å^{-3}) for ubiquitin. Only amides with limited mobility (^{1}H–^{15}N NOE < 0.7) are included. The dashed line represents the best fit between the filled circles and the equation $QCC = A + \sum_i B(\cos\alpha) r_i^{-3}$ where r is the inter-nuclear hydrogen bond distance in ångströms, α is the N–D···O$_i$ angle, $A = 232 \pm 2.3$ kHz, $B = 118 \pm 17$ kHz, and the summation extends over all hydrogen bonding partners of a given amide deuteron. Included in the correlation are 34 D^N QCC values for the amides forming backbone–backbone and backbone–water hydrogen bonds with errors less than 5 kHz. Pearson correlation coefficient is 0.78. Only oxygens for which $\alpha > 140°$ and $r_i < 3$ Å are included in the summation.

lower than average QCC values (e.g. Thr[12], Thr[14], Glu[16], Thr[66] with respective QCC values of 216.4, 210.4, 216.3, 209.7 kHz) — presumably, due to formation of transient hydrogen bonds with water molecules under the conditions of the present study — confirming the absence of significant solvent exchange contributions to the quantified ^{2}H relaxation rates.

2.5. Correlation between D^N QCC and hydrogen bond lengths

According to the empirical parameterization obtained previously by LiWang and Bax from scalar relaxation of the second kind in ubiquitin [11], the amide deuteron QCC is related to hydrogen bond distances as,

$$QCC = A + \sum_i B(\cos\alpha_i) r_i^{-3} \quad (6)$$

where r is the inter-nuclear backbone–backbone hydrogen bond distance in ångströms, α is the N–D···O$_i$ angle, $A = 228 \pm 2.5$ kHz and $B = 130 \pm 21$ kHz, and the summation extends over all hydrogen bonding partners of a given amide deuteron. The QCC values quantified in this work for 34 rigid amides of ubiquitin using Eq. (5) provide a very similar parameterization (Fig. 5b) with $A = 232 \pm 2.3$ kHz and $B = 118 \pm 17$ kHz (Pearson $R = 0.78$). The correlation deteriorates significantly if the second term in Eq. (6) is substituted for $P_2(\cos\alpha)$ where $P_2(x) = (3\cos 2\alpha i - 1)/2$ [11]. It is noteworthy that we have detected statistically significant correlation between D^N QCC and hydrogen bond distances to oxygens of water molecules observed in the X-ray structure of ubiquitin [26]; the QCC values of amides hydrogen-bonded to water molecules (with the exception Gly[47]) are therefore included in Fig. 5b. If these QCC values are removed, the correlation coefficient for the remaining 29 amides increases to 0.82, with $A = 233 \pm 2.3$ kHz, $B = 122 \pm 17$ kHz.

Earlier, using single-crystal solid state NMR measurements Gerald et al. [20] have determined the quadrupole coupling tensor for the amide of the model peptide *N*-acetyl-D,L-valine. Determined in this study is the product $S \times QCC = 212.6$ kHz for a (N–)H···O(=C) distance of 2.32 Å and $\alpha = 159°$, where S is the order parameter of (assumed axially symmetric) fast internal motions. Using Eq. (6) with $A = 232$ and $B = 118$ for this hydrogen bonding distance and angle, we predict a 'static' QCC of 223.3 kHz, yielding the value of $S = 0.95$ — in good agreement with the value of S obtained for quadrupolar interactions by Henry and Szabo [34].

The finite accuracy of crystallographic coordinates in the 1.8 Å-resolution structure of ubiquitin [26] is one of the sources of the scatter in Fig. 5b. The uncertainty in the hydrogen bond lengths is estimated to be about 0.15 Å [11]. This translates into ~15% uncertainty in the parameterization of Eq. (6). However, no improvement in the correlation of Fig. 5b could be achieved when solution structures of ubiquitin, including the 'dynamically refined ensemble' of structures of Vendruscolo and co-workers [35], were used to calculate hydrogen bond distances. It is noteworthy in this context, that other predictors of hydrogen bonding strength in proteins, such as, for example, trans-hydrogen-bond $^{3h}J_{NC'}$ scalar couplings [36] or ^{1}H chemical shift temperature coefficients [37], hardly provide correlations between the measured parameters and hydrogen bond distances that are quantitatively better than the correlation of Fig. 5b and that reported earlier by LiWang and Bax [11].

3. Concluding remarks

In summary, we have shown that the measurements of longitudinal and transverse ^{2}H spin relaxation rates of backbone amide deuterons in [U–^{13}C,^{15}N]-labeled proteins are feasible with an accuracy sufficient for (i) derivation of the global molecular diffusion tensor, and (ii) direct estimation of site-specific D^N QCC values. Although the utility of amide deuterons as probes of backbone dynamics in proteins is compromised by substantial variability of the amide deuteron QCC values from one amide site to another, the estimated site-specific QCC values provide useful information on hydrogen bonding. In agreement with previous (indirect) measurements, the QCC values estimated directly from R_1 and R_2 D^N ^{2}H relaxation rates using the backbone dynamics parameters from ^{15}N relaxation studies, correlate with the inverse cube of the X-ray structure-derived hydrogen bond distances in

ubiquitin: QCC = (232 ± 2.3) + (118 ± 17) $\sum_i(\cos\alpha)r_i^{-3}$ where r is the inter-nuclear hydrogen bond distance in ångströms, and α is the $N-D\cdots O_i$ angle. The measurements described here are intrinsically insensitive and have been performed on a concentrated (3.2 mM) sample of ubiquitin. Therefore, it is unlikely that this methodology can be applied in a routine manner to a wide range of small proteins. Nevertheless, the availability of more sensitive detection devices and higher magnetic field strengths of NMR spectrometers may make such measurements feasible in [U–^{13}C,^{15}N]-labeled proteins with favorable NMR properties in the near future.

Acknowledgments

V.T. thanks the University of Maryland for continuous support. The authors are grateful to Prof. Nikolai Skrynnikov (Purdue University, IN) for the suggestion of exploring amide deuterons as probes of backbone dynamics in proteins and Prof. David Fushman (University of Maryland) for stimulating discussions.

References

[1] A. Abragam, Principles of Nuclear Magnetism, Clarendon Press, Oxford, 1961.
[2] D.R. Muhandiram, T. Yamazaki, B.D. Sykes, L.E. Kay, Measurement of deuterium T_1 and $T_{1\rho}$ relaxation times in uniformly ^{13}C-labeled and fractionally deuterium labeled proteins in solution, J. Am. Chem. Soc. 117 (1995) 11536–11544.
[3] O. Millet, D.R. Muhandiram, N.R. Skrynnikov, L.E. Kay, Deuterium spin probes of side-chain dynamics in proteins. 1. Measurement of five relaxation rates per deuteron in ^{13}C-labeled and fractionally ^{2}H-enriched proteins in solution, J. Am. Chem. Soc. 124 (2002) 6439–6448.
[4] N.R. Skrynnikov, O. Millet, L.E. Kay, Deuterium spin probes of side-chain dynamics in proteins. 2. Spectral density mapping and identification of nanosecond time-scale side-chain motions, J. Am. Chem. Soc. 124 (2002) 6449–6460.
[5] O. Millet, A. Mittermaier, D. Baker, L.E. Kay, The effects of mutations on motions of side-chains in protein L studied by ^{2}H NMR dynamics and scalar couplings, J. Mol. Biol. 329 (2003) 551–563.
[6] V. Tugarinov, J.E. Ollerenshaw, L.E. Kay, Probing side-chain dynamics in high molecular weight proteins by deuterium NMR spin relaxation: an application to an 82-kDa enzyme, J. Am. Chem. Soc. 127 (2005) 8214–8225.
[7] V. Tugarinov, L.E. Kay, A ^{2}H NMR relaxation experiment for the measurement of the time scale of methyl side-chain dynamics in large proteins, J. Am. Chem. Soc. 128 (2006) 12484–12489.
[8] D. Yang, A. Mittermaier, Y.K. Mok, L.E. Kay, A study of protein sidechain dynamics from new ^{2}H auto-correlation and ^{13}C cross-correlation NMR experiments: application to the N-terminal SH3 domain from drk, J. Mol. Biol. 276 (1998) 939–954.
[9] K. Pervushin, G. Wider, K. Wüthrich, Deuterium relaxation in a uniformly ^{15}N-labeled homeodomain and its DNA complex, J. Am. Chem. Soc. 119 (1997) 3842–3843.
[10] D. Sheppard, D.W. Li, R. Brüschweiler, V. Tugarinov, Deuterium spin probes of backbone order in proteins: a ^{2}H NMR relaxation study of deuterated carbon-α sites, J. Am. Chem. Soc. 131 (2009) 15853–15865.
[11] A.C. LiWang, A. Bax, Solution NMR characterization of hydrogen bonds in a protein by indirect measurement of deuterium quadrupole couplings, J. Magn. Reson. 127 (1997) 54–64.
[12] J. Boyd, T.K. Mal, N. Soffe, I.D. Campbell, The influence of a scalar-coupled deuterium upon the relaxation of a ^{15}N Nucleus and its possible exploitation as a probe for side-chain interactions in proteins, J. Magn. Reson. 124 (1997) 61–71.
[13] M. Ikura, L.E. Kay, A. Bax, A novel approach for sequential assignment of ^{1}H, ^{13}C, and ^{15}N spectra of proteins: heteronuclear triple-resonance three-dimensional NMR spectroscopy. Application to calmodulin, Biochemistry 29 (1990) 4659–4667.
[14] A.C. Wang, S. Grzesiek, R. Tschudin, P. Lodi, A. Bax, Sequential backbone assignment of isotopically enriched proteins in D_2O by deuterium-decoupled HA(CA)N and HA(CACO)N, J. Biomol. NMR 5 (1995) 376–382.
[15] J. Xu, O. Millet, L.E. Kay, N.R. Skrynnikov, A new spin probe of protein dynamics: nitrogen relaxation in ^{15}N–^{2}H amide groups, J. Am. Chem. Soc. 127 (2005) 3220–3229.
[16] T.M. Logan, E.T. Olejniczak, R. Xu, S.W. Fesik, Side chain and backbone assignments in isotopically labeled proteins from two heteronuclear triple resonance experiments, FEBS Lett. 314 (1992) 413–418.
[17] P.R. Vasos, J.B. Hall, R. Kummerle, D. Fushman, Measurement of ^{15}N relaxation in deuterated amide groups in proteins using direct nitrogen detection, J. Biomol. NMR 36 (2006) 27–36.
[18] P. Vallurupalli, L.E. Kay, A suite of ^{2}H NMR spin relaxation experiments for the measurement of RNA dynamics, J. Am. Chem. Soc. 127 (2005) 6893–6901.
[19] C.A. Michal, J.C. Wehman, L.W. Jelinski, Deuterium quadrupole-coupling and chemical-shielding tensors in the model dipeptide glycylglycine monohydrochloride monohydrate, J. Magn. Reson. B 111 (1996) 31–39.
[20] R. Gerald II, T. Bernhard, U. Haeberlen, J. Rendell, S. Opella, Chemical shift and electric field gradient tensors for the amide and carboxyl hydrogens in the model peptide *N*-acetyl-D,L-valine. Single-crystal deuterium NMR study, J. Am. Chem. Soc. 115 (1993) 777–782.
[21] M.G. Usha, W.L. Peticolas, R.J. Wittebort, Deuterium quadrupole coupling in *N*-acetylglycine and librational dynamics in solid poly(gamma-benzyl-L-glutamate), Biochemistry 30 (1991) 3955–3962.
[22] J. Chung, E. Oldfield, A. Thevand, L.G. Werbelow, A "magic-angle" sample-spinning nuclear magnetic resonance spectroscopic study of interference effects in the nuclear spin relaxation of polymers, J. Magn. Reson. 100 (1992) 69–81.
[23] G. Lipari, A. Szabo, Model-free approach to the interpretation of nuclear magnetic relaxation in macromolecules: 2. Analysis of experimental results, J. Am. Chem. Soc. 104 (1982) 4559–4570.
[24] G. Lipari, A. Szabo, Model-free approach to the interpretation of nuclear magnetic relaxation in macromolecules: 1. Theory and range of validity, J. Am. Chem. Soc. 104 (1982) 4546–4559.
[25] D.E. Woessner, Nuclear spin relaxation in ellipsoids undergoing rotational Brownian motion, J. Chem. Phys. 37 (1962) 647–654.
[26] S. Vijay-Kumar, C.E. Bugg, W.J. Cook, Structure of ubiquitin refined at 1.8 ångströms resolution, J. Mol. Biol. 194 (1987) 531–544.
[27] C.H. Cho, J. Urquidi, S. Singh, G.W. Robinson, Thermal offset viscosities of liquid H_2O, D_2O and T_2O, J. Phys. Chem. B 103 (1999) 1991–1994.
[28] J.P. Jacobsen, H.K. Bildsoe, K. Schaumburg, Application of density of matrix formalism in NMR spectroscopy. II. The one-spin-1 case in anisotropic phase, J. Magn. Reson. 23 (1976) 153–164.
[29] G.P. Connelly, Y. Bai, M.F. Jeng, S.W. Englander, Isotope effects in peptide group hydrogen exchange, Proteins 17 (1993) 87–92.
[30] Y. Bai, J.S. Milne, L. Mayne, S.W. Englander, Primary structure effects on peptide group hydrogen exchange, Proteins 17 (1993) 75–86.
[31] L.E. Kay, D.A. Torchia, A. Bax, Backbone dynamics of proteins as studied by ^{15}N inverse detected heteronuclear NMR spectroscopy: application to staphylococcal nuclease, Biochemistry 28 (1989) 8972–8979.
[32] N. Tjandra, S.E. Feller, R.W. Pastor, A. Bax, Rotational diffusion anisotropy of human ubiquitin from ^{15}N NMR relaxation, J. Am. Chem. Soc. 117 (1995) 12562–12566.
[33] R. Brüschweiler, Normal modes and NMR order parameters in proteins, J. Am. Chem. Soc. 114 (1992) 5341–5344.
[34] E.R. Henry, A. Szabo, Influence of vibrational motion on solid state line shapes and NMR relaxation, J. Chem. Phys. 82 (1985) 4753–4761.
[35] K. Lindorff-Larsen, R.B. Best, M.A. Depristo, C.M. Dobson, M. Vendruscolo, Simultaneous determination of protein structure and dynamics, Nature 433 (2005) 128–132.
[36] G. Cornilescu, B.E. Ramirez, M.K. Frank, G.M. Clore, A.M. Gronenborn, A. Bax, Correlation between $^{3h}J_{NC'}$ and hydrogen bond length in proteins, J. Am. Chem. Soc. 121 (1999) 6275–6279.
[37] N.J. Baxter, M.P. Williamson, Temperature dependence of ^{1}H chemical shifts in proteins, J. Biomol. NMR 9 (1997) 359–369.
[38] A.J. Shaka, J. Keeler, T. Frenkiel, R. Freeman, An improved sequence for broadband decoupling: WALTZ-16, J. Magn. Reson. 52 (1983) 335–338.
[39] L.E. Kay, M. Ikura, R. Tschudin, A. Bax, Three-dimensional triple-resonance NMR spectroscopy of isotopically enriched proteins, J. Magn. Reson. 89 (1990) 496–514.
[40] H. Geen, R. Freeman, Band-selective radiofrequency pulses, J. Magn. Reson. 93 (1991) 93–141.
[41] S.L. Patt, Single- and multiple-frequency-shifted laminar pulses, J. Magn. Reson. 96 (1992) 94–102.
[42] J. Boyd, N. Soffe, Selective excitation by pulse shaping combined with phase modulation, J. Magn. Reson. 85 (1989) 406–413.
[43] D. Marion, M. Ikura, R. Tschudin, A. Bax, Rapid recording of 2D NMR spectra without phase cycling. Application to the study of hydrogen exchange in proteins, J. Magn. Reson. 85 (1989) 393–401.
[44] F. Delaglio, S. Grzesiek, G.W. Vuister, G. Zhu, J. Pfeifer, A. Bax, NMRPipe: a multidimensional spectral processing system based on UNIX pipes, J. Biomol. NMR 6 (1995) 277–293.
[45] U. Kamith, J.W. Shriver, Characterization of the thermotropic state changes in myosin subfragment-1 and heavy meromyosin by UV difference spectroscopy, J. Biol. Chem. 264 (1989) 5586–5592.
[46] J. Abildgaard, P.E. Hansen, M.N. Manalo, A. LiWang, Deuterium isotope effects on ^{15}N backbone chemical shifts in proteins, J. Biomol. NMR 44 (2009) 119–126.